ROTATIONAL SLIDING OF 3D STEEL FRAME EQUIPPED WITH PASSIVE FRICTION DAMPERS AT BASE WITH ECCENTRICITY

H. Miyamoto[1], M. Takiguchi[2], M. Yamanari[3]

[1] *Graduate Student, Graduate School of Science of Sci. and Tech., Kumamoto University, 194d8442@st.kumamoto-u.ac.jp*
[2] *Graduate Student, Graduate School of Science of Sci. and Tech., Kumamoto University, 191d8421@st.kumamoto-u.ac.jp*
[3] *Prof., Faculty of Advanced Sci. and Tech., Kumamoto University, yamanari@kumamoto-u.ac.jp*

Abstract

This research is concerned with a new vibration control system with passive friction dampers at the base of a building. The behavior of a 3D steel frame with eccentricity in plan and equipped the passive friction damper system under strong ground motions is described in this paper. The passive friction damper system has both functions of the base-isolation and the damping against the earthquake. The building attacked by strong ground motions will slide because the column-bases of the first floor are not tied to the foundation. The behavior causes that the seismic force inputted to the superstructure can be reduced as well as the seismic energy can be dissipated on the friction surface. Previous studies investigated the seismic response characteristics of 2D steel frames equipped with friction dampers at the base. However, this study deals with the analysis of 3D steel frames equipped with the friction dampers at the base. The purpose of this is to obtain the basic information on the seismic response of a 3D steel frame to which this vibration control system is applied.

When the superstructure has stiffness eccentricity in its plan, not only translational slide, but rotational slide occurs at the base. It is supposed that the torsional response generated in the superstructure due to eccentricity causes the rotational slide of the damper layer. The friction damper system has no restoring mechanism. Therefore, a suitable clearance between the building and the retaining wall shall be required to avoid the collision. When the translational and rotational slide occur simultaneously, a larger clearance must be required more than when only translational slide occurs. For this reason, it is important to evaluate each sliding displacement quantitatively. In the seismic analysis in this paper, the predominant period of the input wave and the peak ground velocity are used as analytical parameters. The relationship between their parameters and sliding displacement is discussed.

The slide phenomenon of the friction damper system has a rigid-plastic type hysteresis characteristic. Horizontal springs were applied under the column bases at the first story in order to reproduce the characteristic. Their horizontal springs have a perfect elastic-plastic type restoring force characteristic with an extremely large initial stiffness. The slip resistance of the friction damper is expressed by the product of the slip coefficient and the contact force. When a horizontal force reaching the slip resistance inputs to the friction damper, the horizontal spring yields and deforms while keeping the slip resistance. The deformation of the horizontal springs represents the sliding displacement of the friction damper system.

The slip coefficient of the friction damper system was set to 0.05, 0.20, and 0.35. In addition, the natural period of the frame was set three types with changing the initial stiffness of the columns and the beams. It is expected that the torsional response of the superstructure would change due to the change of the slip coefficient and the natural period. This paper also describes the relationship between the torsional response of the superstructure and the sliding displacement.

Keywords: Seismic analysis; Passive friction damper; Eccentricity

1. Introduction

Previous researches have been proposing the vibration control system equipped with passive friction dampers at the base of the building hereinafter referred to as “Column-base friction damper system” [1, 2]. Fig. 1 shows an image of the Column-base friction damper system. The building under a strong earthquake will laterally slide because the column bases of the first floor are not tied to the foundation. The behavior causes that the seismic force inputted to the superstructure can be reduced as well as the seismic energy can be dissipated on the friction surface. It must be remembered that the Column-base friction damper system has no restoring mechanism. Therefore, it is important to quantitatively evaluate the sliding displacement for obtaining enough clearance against the retaining walls and for designing the flexible joints of such as the gas and water pipeline. It has been clarified that when a steel frame with the Column-base friction damper system has eccentricity, rotational slide phenomenon occurs [3]. Fig. 2 shows the mechanism of the rotational slide phenomenon. In addition to the slide in the input direction of the seismic wave that is translational slide, the rotational slide occurs by the torsional response of the superstructure. There is a possibility that the sliding displacement increases by the rotational slide as compared with the case of only translational slide. It is necessary to quantitatively evaluate the translational slide and the rotational slide.

This study focuses on the predominant period of seismic waves and the peak ground velocity as a preliminary study for quantitative evaluation of sliding displacement. The aim of the study is to qualitatively evaluate the relationship between them and each sliding displacement. The seismic analysis was performed using the predominant period of the seismic wave and the maximum ground velocity as parameters.

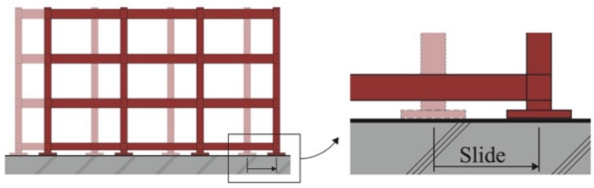

Fig. 1 – Column-base friction damper system

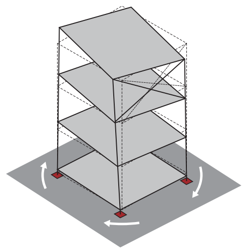

Fig. 2 – Mechanism of the rotational slide phenomenon

2. Analytical model

2.1 Friction damper

The Column-base friction damper in the seismic response analysis is modelled as shown in Fig. 3. The slide phenomenon of the Column-base friction damper system has a rigid-plastic type hysteresis characteristic. Horizontal springs were applied to the first story column bases in order to reproduce the characteristic. The horizontal spring has a perfectly elastic-plastic type restoring force characteristic with an extremely large initial stiffness K_h (Fig. 3 (b)). u represents the sliding displacement of the column base. The slip resistance F_s is defined by Eq. (1) based on the Coulomb's friction law. And it is obtained from the product of slip coefficient μ and contact force W. Here, it is assumed that the slip coefficient is constant of whether it is static or dynamic.

$$F_s = \mu\, W \tag{1}$$

(a) Horizontal spring (b) Hysteresis characteristic

Fig. 3 – Analytical model of the Column-base friction damper

2.2 Frame for Analysis

Table 1 shows the designations of the frames for analysis, Table 2 shows the story weights and sectional dimension of the members, Table 3 shows the natural period of each frame and Fig. 4 shows the dimensions of the frame. Fig. 5 shows the first and second eigen modes. The slip coefficient of the Column-base friction damper was set to 0.05, 0.20, and 0.35, and the natural period of the frame was set 3 types by changing the initial stiffness of the columns and beams. Therefore, the seismic analysis was performed on 9 types frames as shown in Table 1 (a). The changes in the bending stiffness and the shear stiffness of the columns and the beams are summarized in Table 1 (b). The initial stiffness of each frame was changed by multiplying the initial stiffness of the original frame (Initial stiffness magnification: 1.00) by the initial stiffness magnification as shown in Table 1 (b). Because of this, the natural period was changed. Their 9 types frame are all the same as shown in Fig. 1, and the story weights and sectional dimension of members are all the same as shown in Table 2. The information on only the Y direction is shown in Table 3 and Fig. 5. since the input direction of the seismic waves were only the Y direction in Fig. 4.

Table 1 (a) – Designation of frame

	μ =0.05	μ =0.20	μ =0.35
Index of initial stiffness magnification：O	Frame O – 0.05	Frame O – 0.20	Frame O – 0.35
Index of initial stiffness magnification：A	Frame A – 0.05	Frame A – 0.20	Frame A – 0.35
Index of initial stiffness magnification：B	Frame B – 0.05	Frame B – 0.20	Frame B – 0.35

Table 1 (b) – Initial stiffness magnification

Index of initial stiffness magnification	Column		beam
	Bending stiffness	Shear stiffness	Bending stiffness
O	1.00	1.00	1.00
A	0.60	0.60	0.60
B	0.30	0.30	0.30

Table 2 – Weight and sectional dimension

Story	Weight (kg)	Sectional dimension (mm)	
		Column	Beam
	24688	□-300x300x16.0x56.0	H-500x200x10.0x16.0x13.0
3	25483		
2	25483		
1	25483		

Table 3 – Natural period of frame

Designation of frame	Natural period (s)	
	First (Y direction)	Second (Y direction)
Frame O – 0.05, Frame O – 0.20, Frame O – 0.35	0.489	0.361
Frame A – 0.05, Frame A – 0.20, Frame A – 0.35	0.628	0.458
Frame B – 0.05, Frame B – 0.20, Frame B – 0.35	0.906	0.672

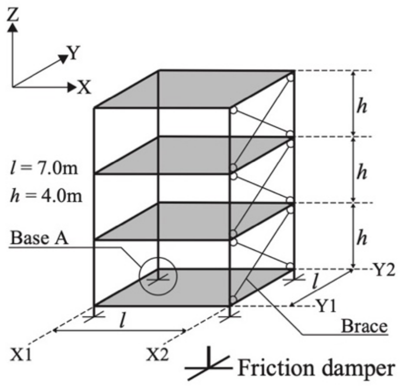

Fig. 4 – Dimension of the frame

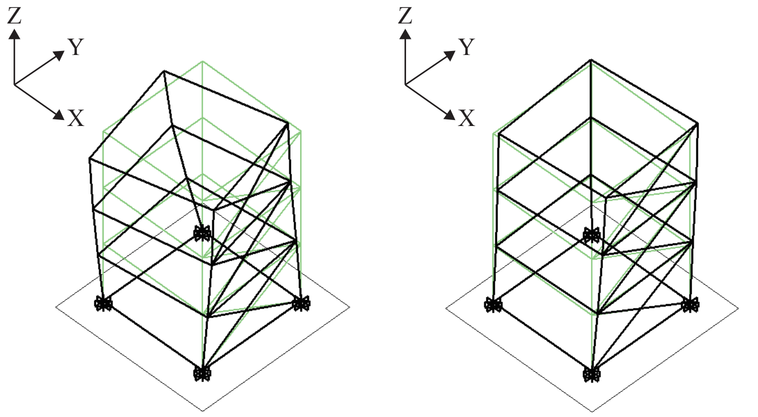

(a) First (Y direction)

(b) Second (Y direction)

Fig. 5 – Eigen mode

This paper deals with the frames with eccentricity (stiffness eccentricity) due to planar unequal distribution of horizontal stiffness. In order to generate stiffness eccentricity, the braces are equipped only on one side (X2 frame) of the frame parallel to the seismic wave input direction (Y direction in Fig. 1). For evaluation of eccentricity, the Japanese design index, Eccentricity ratio R_e is used. It is defined by Eq. (2) and calculated for each story. e is the eccentric distance and r_e is the elastic radius of a plan. Not only the horizontal stiffness in the seismic wave input direction but also the horizontal stiffness in the orthogonal direction are considered by using the index of the elastic radius. Under the Japanese design standard, small and medium-sized buildings generally have the eccentricity ratio of 0.15 or less. For example, a frame with the eccentricity ratio of 0.30 can be evaluated as a frame with a relatively large eccentricity. Table 4 shows the eccentricity ratio of each frame. Their values are about 0.30. The brace was designed so that all frames have almost the same stiffness ratio. Here, one of the factors of eccentricity is due to unequal distribution of mass. In this study, in order to evaluate only the effect of stiffness eccentricity, a virtual brace whose weight is almost zero is used for the analysis. Therefore, the center of gravity does not move by the braces, only the center of rigidity moves. The dead and the live loads were distributed on each floor.

Changes in slip coefficient and natural period are expected to change in the torsional response of the superstructure. In this paper, the predominant period of the seismic wave and the peak ground velocity are used as analysis parameters. The relationship between their parameters and the sliding displacement of each frame was investigated.

$$R_e = e / r_e \tag{2}$$

Table 4 – Eccentricity ratio R_e of each frame

Story	Frame O – 0.05 Frame O – 0.20 Frame O – 0.35	Frame O – 0.05 Frame A – 0.20 Frame B – 0.35	Frame B – 0.05 Frame B – 0.20 Frame B – 0.35
3	0.302	0.301	0.302
2	0.303	0.303	0.301
1	0.303	0.302	0.300

3. Method and condition of analysis

The static structural analysis program SEIN La CREA (ver. 3.0) and the three-dimensional inelastic dynamic analysis program SEIN La DANS (ver. 3.0) were used for the numerical investigation. The Newmark-β (β = 1/4) method is used for numerical integration, and the incremental time is 0.0001 s. The type of the damping is Rayleigh damping, and both the first and the second damping constants are 2 %. The Beam-end rigid-plastic spring model is used for columns and beams, and the strain hardening is not considered. Note that, no yielding occurred in all members of the superstructure in the seismic analysis of this paper. In order to prevent changing the Eccentricity ratio due to the buckling and yielding of the brace, the analytical conditions were set so that the braces do not occur buckling and yielding. The input direction of the seismic wave is the Y direction in Fig. 4. Table 5 shows the input waves. In this study, the predominant period of the seismic wave and the peak ground velocity (PGV) are used as analysis parameters. Harmonic waves with periods which changed from 0.2 s to 2.0 s in increments of 0.2 s, a couple of artificial earthquake waves, and four observed earthquake waves were used as input waves. The predominant periods of the simulated earthquake waves and observed earthquake waves were determined from the Acceleration Fourier amplitude spectrum of each wave as shown in Fig. 6. The period in which the Acceleration Fourier amplitude spectrum shows the maximum value in the range of 0.0 s $<$ T $\leqq$ 1.0 s, which is expected to have a large effect on the seismic response of the frame, is defined as the predominant period. The relationship between the sliding displacement and the predominant period as characteristic value of each input wave was investigated. The peak ground acceleration (PGA) was adjusted so that the peak ground velocity was 0.75 m/s in the seismic analysis using the predominant period as a parameter. The peak ground velocity (PGV) was changed from 0.2 m/s to 1.6 m/s in increments of 0.2 m/s in the seismic analysis using the PGV as an analytical parameter. The representative period of the sine wave takes 1.0 s. The relationship between the sliding displacement and the PGV was investigated.

Table 5 – (a) Input waves and predominant period

Input waves	Predominant period (s)	PGV (m/s)	PGA (m/s^2)	Duration (s)
Sine wave -T=0.2s	0.2	0.75	2562.3	0.0-20.0
Sine wave -T=0.4s	0.4		1187.9	
Sine wave -T=0.46	0.6		792.6	
Sine wave -T=0.8s	0.8		590.3	
Sine wave -T=1.0s	1.0		472.8	
Sine wave -T=1.2s	1.2		393.1	
Sine wave -T=1.4s	1.4		337.2	
Sine wave -T=1.6s	1.6		294.7	
Sine wave -T=1.8s	1.8		262.1	
Sine wave -T=2.0s	2.0		235.7	
BCJ-L2	0.52		331.8	0.0-60.0
Seismic wave in notification (random phase)	0.73		421.7	
El Centro (1940) NS	0.68		765.0	0.0-20.0
JMA Kobe (1995) NS	0.88		674.9	
NTT Kobe (1995) NS	0.98		285.3	
Taft (1952) EW	0.83		745.3	

Table 5 – (b) Input waves and peak ground velocity (PGV)

Input waves	PGV (m/s)	PGA (m/s²)	Duration (s)
Sine wave -T=1.0s	0.2, 0.4, …, 1.4, 1.6	1.26, 2.52, …, 8.83, 10.1	0.0-20.0
BCJ - L2		0.89, 1.77, …, 6.19, 7.08	0.0-60.0
Seismic wave in notification (random phase)		1.12, 2.25, …, 7.87, 9.00	
El Centro (1940) NS		2.04, 4.08, …, 14.3, 16.3	0.0-20.0
JMA Kobe (1995) NS		1.80, 3.60, …, 10.8, 12.6	0.0-20.0
NTT Kobe (1995) NS		0.76, 1.52, …, 5.33, 6.09	0.0-20.0
Taft (1952) EW		1.99, 3.98, …, 13.9, 15.9	0.0-20.0

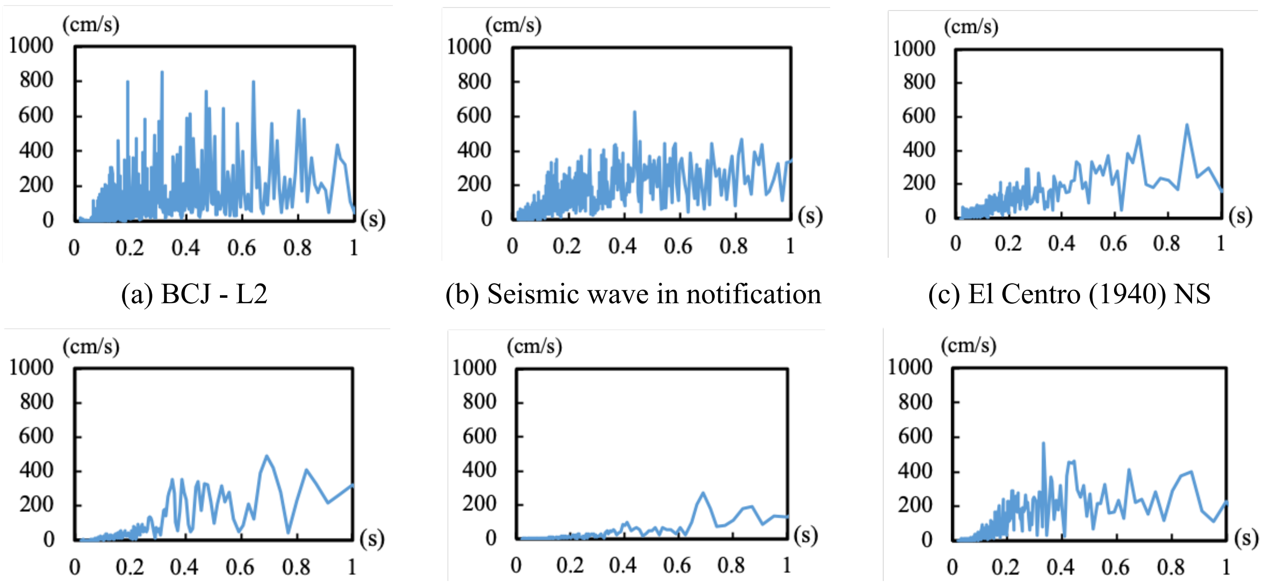

(a) BCJ - L2 (b) Seismic wave in notification (c) El Centro (1940) NS

(d) JMA Kobe (1995) NS (e) NTT Kobe (1995) NS (f) Taft (1952) EW

Fig. 6 – Acceleration Fourier amplitude spectrum of input waves

4. Analysis results

4.1 Definition of sliding displacement

In order to evaluate the effect of stiffness eccentricity on the slide phenomenon, the translational sliding displacement u_t, the rotational sliding displacement u_r, and the sliding displacement u as shown in Fig. 7 were defined as indexes. The translational sliding displacement is the pure sliding displacement along the direction of ground motion. On the other hand, the rotational sliding displacement is caused by rotation around the center of rigidity of the plan, and it is independent of translational sliding displacement. This paper focuses on the rotational sliding displacement of the column base A shown in Figs. 4 and 7. The relationship between the stiffness eccentricity and slide phenomenon was quantitatively evaluated with respect to the maximum value of each index.

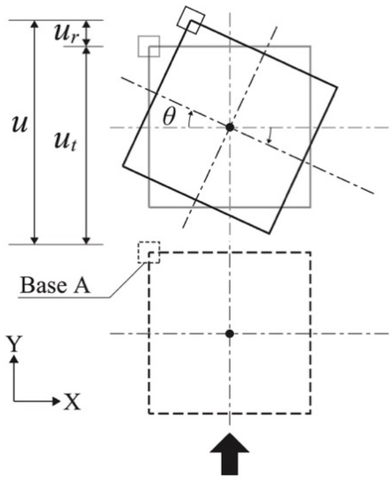

Fig. 7 – Definition of sliding displacement

4.2 Relationship predominant period of input wave and sliding displacement

This section describes the relationship between the predominant period of each input wave and the sliding displacement defined in the previous chapter.

4.2.1 Maximum rotational sliding displacement

Fig. 8 shows the relationship between the period T_s of the sine wave and the maximum rotational sliding displacement $u_{r\,max}$. The frame has the slip coefficient of 0.05, the maximum rotational sliding displacement was almost constant regardless of the period of the sine wave. In addition, the maximum rotational sliding displacement of the frame was smaller than those of almost other frames which set larger slip coefficient. It is assumed that the torsional response of the superstructure became small because the seismic force input to the superstructure was small, consequently the rotation sliding hardly occurs. A large rotational sliding displacement occurred in Frame B – 0.35 under the sine wave with the period of 1.6 s. However, the period was different from the natural period of the frame. Now, the Column-base friction damper system is expected to respond to the earthquake like conventional frame with column bases fixed when the frame is static. However, the frame slides constantly when the slip coefficient is small, so it is difficult to grasp the seismic response. This problem needs further study in the future. In the frames set slip coefficient of 0.20 and 0.35, the large rotational sliding displacement was generated by the sine waves with a period close to the natural period of the frame. The correlation between the natural period of the frame and the period of sine wave could not be confirmed for Frame B, although the rotational sliding displacement tended to increase as the sine wave around a certain period as in other frames. In addition, the period at which the maximum rotational sliding displacement peaks becomes shorter as the slip coefficient increases.

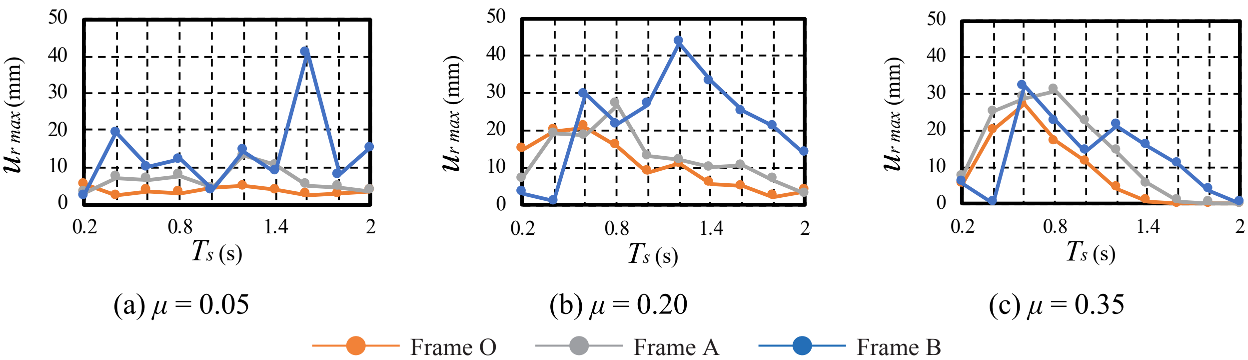

Fig. 8 – Relationship period of sine wave and maximum rotational sliding displacement

Fig. 9 shows the relationship between the predominant period T_p of the seismic wave and the maximum rotational sliding displacement $u_{r\ max}$. The predominant period was used as the characteristic value of each seismic wave, although no significant correlation was found between the predominant period and the maximum rotational sliding displacement. On the other hand, it should be noted that the seismic wave generating the largest maximum rotational sliding displacement depends on the slip coefficient and the natural period of the frame. For example, focusing on the results of Frame O, the largest maximum rotational sliding displacement is generated by BCJ - L2 when the slip coefficient takes 0.20, however it is generated by El Centro (1940) NS when the slip coefficient takes 0.35. It suggests that it is difficult to evaluate the sliding behavior of the Column-base friction damper system only by earthquake phase. Further studies are needed in order to clarify the effects of earthquake phase on different slip coefficients and natural period.

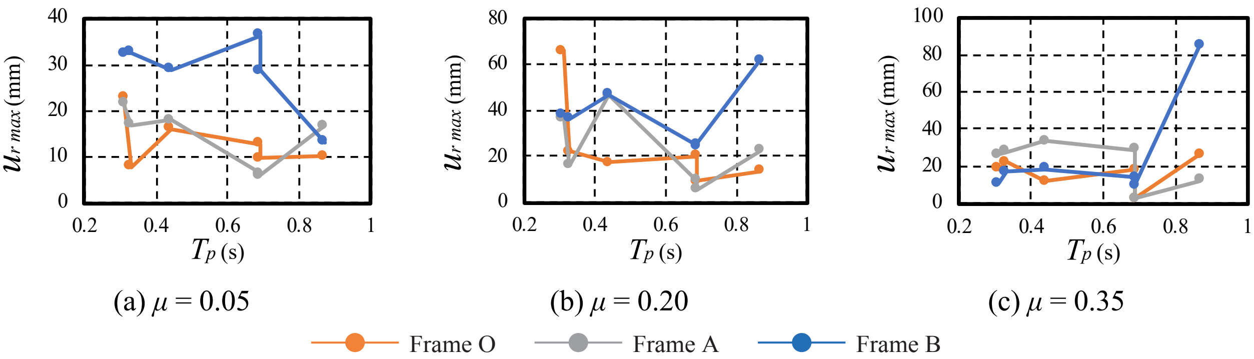

Fig. 9 – Relationship predominant period of seismic wave and maximum rotational sliding displacement

4.2.2 Maximum translational sliding displacement

Fig. 10 shows the relationship between the period T_s of the sine wave and the maximum translational sliding displacement $u_{t\ max}$. The maximum translational sliding displacement tended to increase as the period of the sine wave become longer in a frame with the slip coefficient of 0.05. On the other hand, in frames with the slip coefficient of 0.20 and 0.35, the maximum translational sliding displacement tended to increase as the period of the sine wave approaches a certain one. The period of the sine wave when the maximum translational sliding displacement reaches its peak is close to the natural period of each frame in most of the cases. It is inferred that translational sliding displacement increases because of the resonance phenomenon of the frame as with the above-mentioned trend of the maximum rotational sliding displacement.

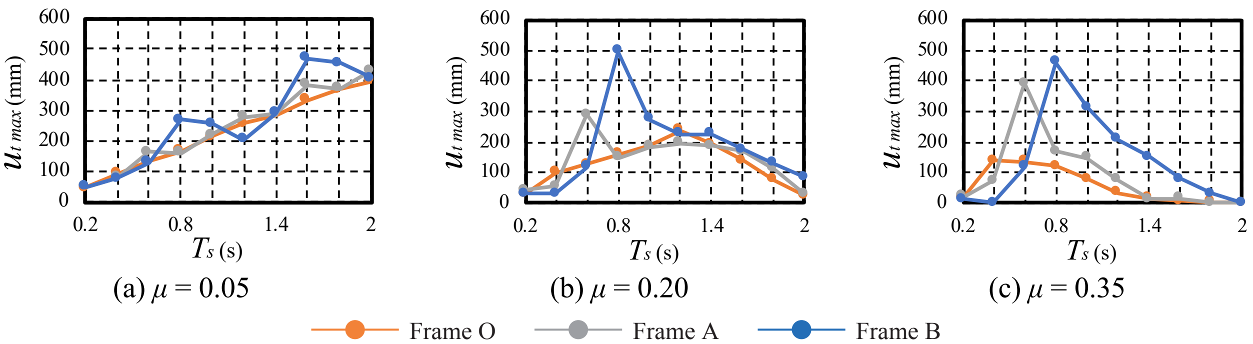

Fig. 10 – Relationship period of sine wave and maximum translational sliding displacement

Fig. 11 shows the relationship between the predominant period T_p of the seismic wave and the maximum translational sliding displacement $u_{t\ max}$. No significant correlation was found between the predominant period of the seismic wave and the maximum translational sliding displacement. The sliding behavior generated by each seismic wave differs because of difference of the slip coefficient and the natural period as with the above-mentioned behavior of the maximum rotational sliding displacement.

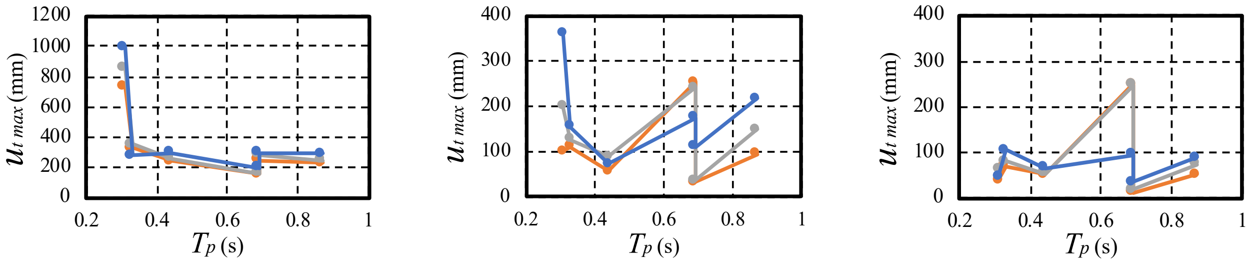

(a) $\mu = 0.05$ (b) $\mu = 0.20$ (c) $\mu = 0.35$

Frame O Frame A Frame B

Fig. 11 – Relationship predominant period of seismic wave and maximum translational sliding displacement

4.3 Relationship peak ground velocity of input wave and sliding displacement

This section describes the relationship between the peak ground velocity of each input wave and the sliding displacement.

4.3.1 Maximum rotational sliding displacement

Fig. 12 shows the relationship between the maximum ground velocity PGV of the input wave and the maximum rotational sliding displacement $u_{r\,max}$. The maximum rotational sliding displacement generated by each seismic wave almost increases with an increase of the maximum ground velocity. However, its displacement becomes sometimes the its displacement sometimes decreases although the maximum ground velocity increases. Fig. 13 shows the change of the rotational sliding displacement when the seismic wave in notification is input in Frame A – 0.20. Their graphs mean the results of parts where the Maximum rotational sliding displacement changes from increase to decrease in Fig. 12 [c] - (b). Fig. 13 can be seen that the displacement to the negative direction gradually increases. The natural period of the frame and the earthquake phase make a difference of the sliding behavior. In addition, the maximum rotational sliding displacement increases as the slip coefficient is larger in most of the cases.

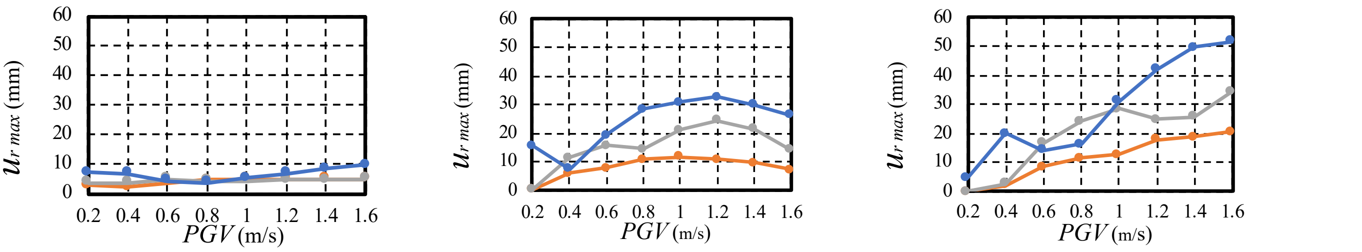

(a) $\mu = 0.05$ (b) $\mu = 0.20$ (c) $\mu = 0.35$

[a] Sinewave -T=1.0s

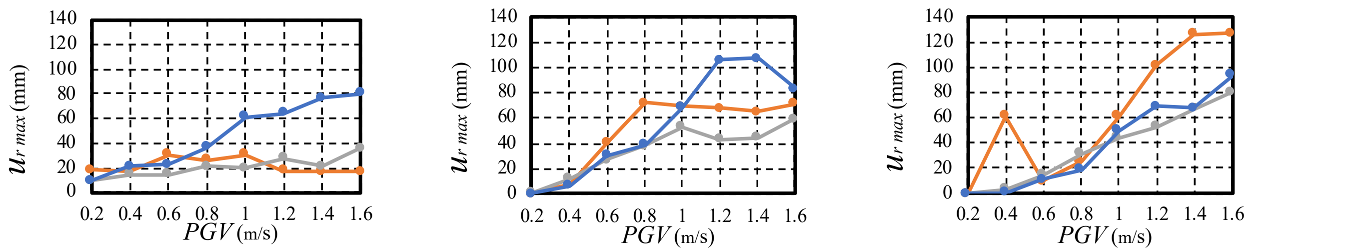

(a) $\mu = 0.05$ (b) $\mu = 0.20$ (c) $\mu = 0.35$

[b] BCJ-L2

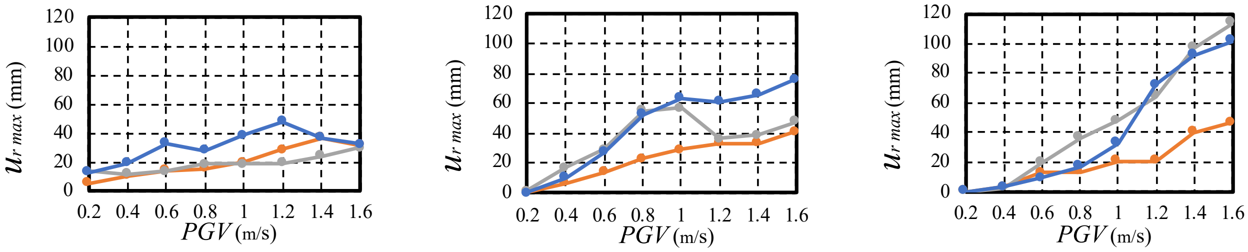

(a) $\mu = 0.05$ (b) $\mu = 0.20$ (c) $\mu = 0.35$

[c] Seismic wave in notification

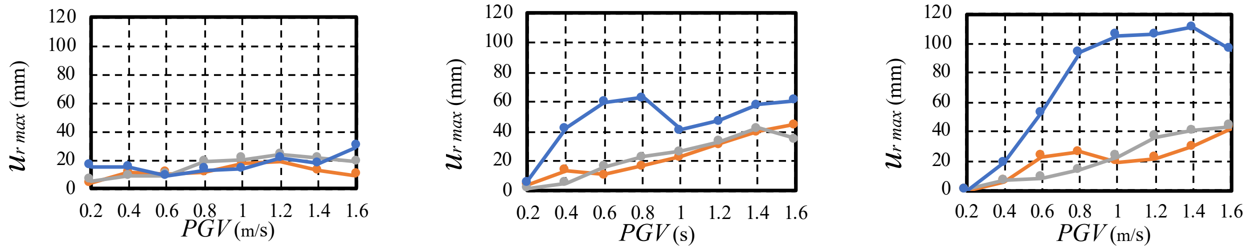

(a) $\mu = 0.05$ (b) $\mu = 0.20$ (c) $\mu = 0.35$

[d] El Centro (1940) NS

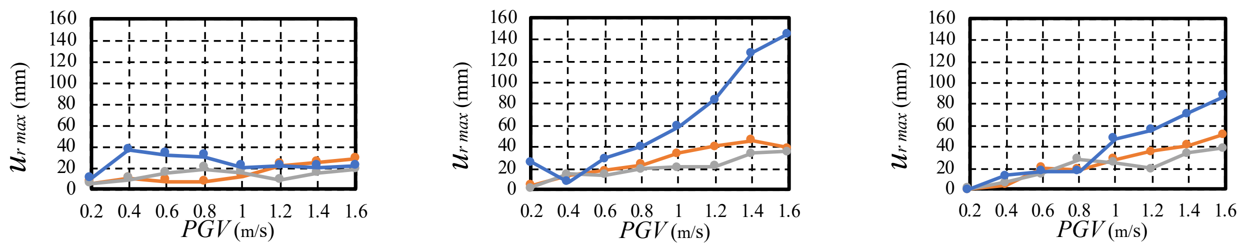

(a) $\mu = 0.05$ (b) $\mu = 0.20$ (c) $\mu = 0.35$

[g] Taft (1952) EW

Fig. 12 – Relationship between PGV of each input wave and the maximum rotational sliding displacement

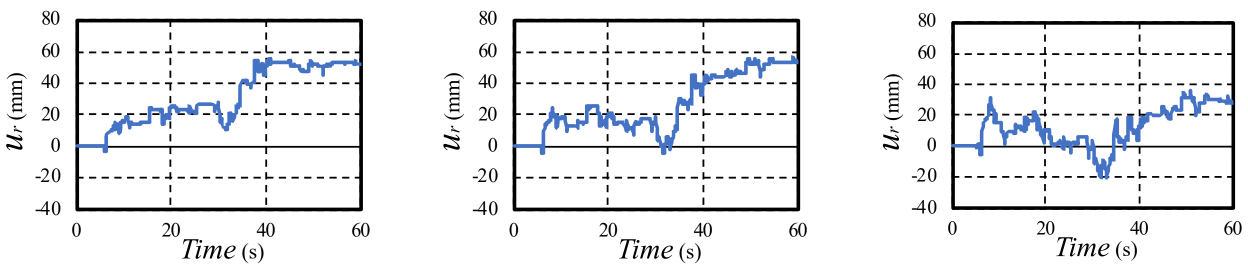

(a) PGV = 0.8 (m/s) (b) PGV = 1.0 (m/s) (c) PGV = 1.2 (m/s)

Fig. 13 – Transient analysis results of the rotational sliding displacement (Frame A – 0.20)

4.3.2 Maximum translational slidings displacement

Fig. 14 shows the relationship between the peak ground velocity *PGV* of the input wave and the maximum translational sliding displacement $u_{t\,max}$. The maximum rotational sliding displacement generated by each seismic wave almost increases with an increase of the peak ground velocity. The same is true of the maximum rotational sliding displacement, although the maximum translational sliding displacement tended to increase monotonically with the peak ground velocity in most of the cases. The translational sliding displacement is larger for the frame whose the natural period is longer in most of the cases. It is inferred that this reason is due to the large seismic response of the superstructure whose stiffness is lower. Furthermore, the maximum translational sliding displacement is small when the slip coefficient is small in many cases. That trend was opposite to the above-mentioned trend of the maximum rotational sliding displacement. Only some results for a part of input waves were shown due to space limitations. The same trend was found for all input waves.–There is a possibility that maximum translational sliding displacement increases significantly with an increase of the peak ground velocity. It is extremely unlikely that strong ground motions whose peak ground velocity is 1.6 m/s occur, although the sliding displacement must be controlled.

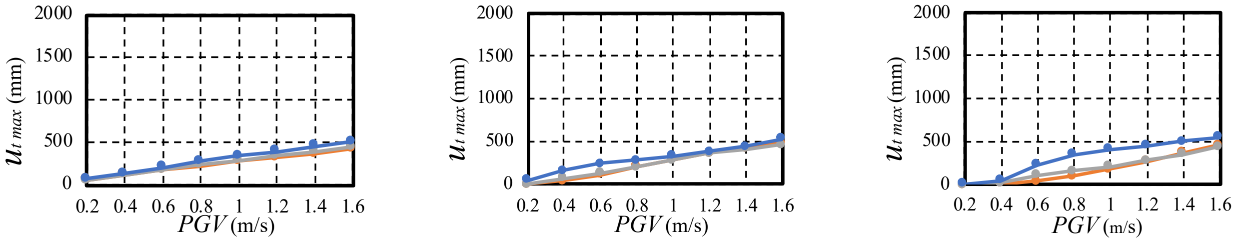

(a) $\mu = 0.05$ (b) $\mu = 0.20$ (c) $\mu = 0.35$

[a] Sinewave -T=1.0s

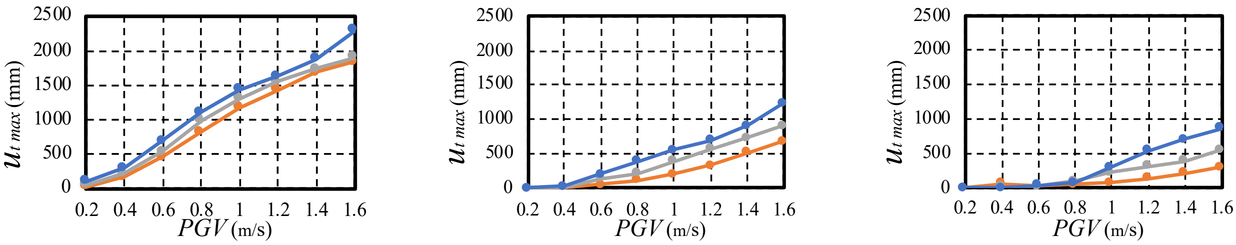

(a) $\mu = 0.05$ (b) $\mu = 0.20$ (c) $\mu = 0.35$

[b] BCJ-L2

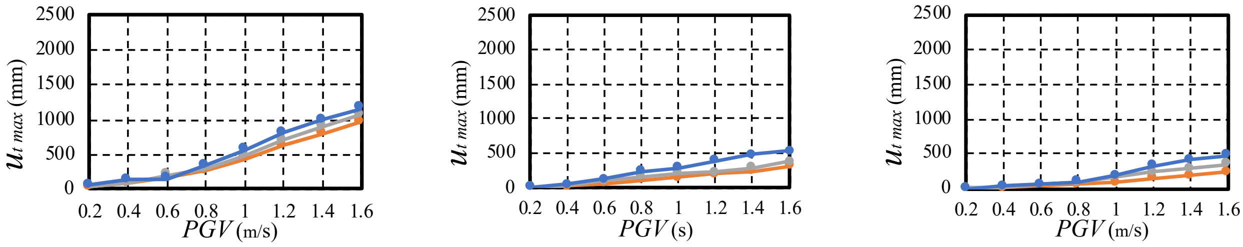

(a) $\mu = 0.05$ (b) $\mu = 0.20$ (c) $\mu = 0.35$

[c] El Centro (1940) NS

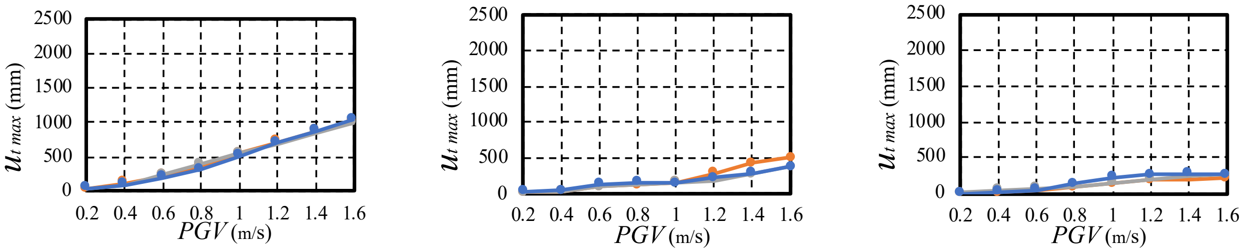

(a) $\mu = 0.05$ (b) $\mu = 0.20$ (c) $\mu = 0.35$

[d] Taft (1952) EW

Frame O Frame A Frame B

Fig. 14 – Relationship between PGV of each input wave and the maximum translational sliding displacement

5. Conclusions

In this study, seismic response analysis of three-dimensional steel frame with stiffness eccentricity used the column-base friction damper system was performed. As a result, the following behaviors regarding rotational slide and translational slide were clarified.

[1] There is a possibility that both the rotational sliding displacement and the translational sliding displacement increase when the superstructure has a natural period which close to the predominant period of the seismic wave. It is assumed that the increase is because of the resonance phenomenon of the superstructure.

[2] There is a possibility that both the rotational sliding displacement and the translational sliding displacement increase as the peak ground velocity increases. However, there are exceptions in the case of the rotation slide. The natural period of the frame and the earthquake phase make a difference of the slide behavior.

[3] There is a possibility that the rotational sliding displacement is large when the slip coefficient is large. On the other hand, the translational sliding displacement is small when the slip coefficient is large in most cases. The magnitude of the rotational sliding displacement depends on the magnitude of the torsional response of the superstructure. Therefore, it is assumed that the rotational sliding displacement increases because the torsional response of the superstructure increases when the slip coefficient is large.

6. References

[1] Nakamura R, Aramaki R, Jin C, Yamanari M (2014): Dynamic behavior of partially base-isolated steel frames with friction dampers (Part 1 - Comparison between seismic behaviors of fully isolated and partially isolated frames). *Architectural Institute of Japan*, 437 - 440.

[2] You T, Hirata D, Yamanari M (2018): Dynamic response behavior of 3D steel frame with passive friction dampers at base. *Proceedings of Constructional Steel, Vol.26* ,615-620

[3] Miyamoto H, Takiguchi M, Liu J, Yamanari M (2019): BEHAVIOR OF PASSIVE FRICYION DAMPERS AT FOUNDATION OF 3D STEEL FRAME WITH ECCEBTRICITY. *12th Pacific Structural Steel Conference*, Tokyo, Japan.

